

A mini-review on proton conduction of BaZrO₃-based perovskite electrolytes

¹SATCHIDANANDA GHOSH, *Gandhi Institute of Excellent Technocrats, Bhubaneswar, India*

²RABI NARAYAN SAHOO, *Gopal Krishna College of Engineering and Technology, Koraput, Odisha, India*

Abstract

Proton conducting ceramics show promise in fuel cells, electrolyzers, permeation membranes, sensor applications, and membrane reactors. Among several types of materials that exhibit proton conduction, perovskite oxides show high proton conductivity at intermediate temperatures, presenting potential benefits for long-term use and lower costs for energy applications. Doped barium zirconate, BaZrO₃, is a material that has shown high proton conductivity with encouraging chemical stability. Therefore, it is considered a promising material especially for proton-conducting solid oxide electrochemical cells. Although the proton conduction of doped BaZrO₃ has been extensively characterized, the specific phenomena behind its proton conduction are not fully understood. Only recently have specialized techniques and computational tools begun to elucidate the phenomena that determine the conduction properties of the material. In this mini review, an evaluation of the factors affecting the proton conductivity of doped BaZrO₃ perovskites and the phenomena governing variations in proton concentration and mobility are presented. Special attention is given to proton interactions with dopants and their resulting effect on hydration and transport properties. Technical strategies are provided to give some guidance on the development of protonic ceramics in energy conversion applications.

Keywords: proton conductor, perovskite ceramics, hydration thermodynamics, proton concentration, proton trapping, solid oxide cells

1. Introduction

The interest in proton-conducting ceramics has continuously grown since the 1980s when proton conduction was first observed in doped SrCeO₃ oxides at high temperatures (>600 °C) in a humidified atmosphere [1, 2]. Later on, some new materials such as niobates [3], tantalates [3], perovskites, and disordered perovskites [4, 5], were shown to exhibit proton conductivity. Each material family demonstrated its own special characteristics, requiring a deeper understanding of each to optimize proton conduction for a given application. The applications of proton-conducting ceramics are diverse: sensors, hydrogen separation membranes, fuel cells, steam electrolyzers, and membrane reactors [6–11]. In particular, there has been significant recent interest in their use in solid oxide electrolysis cells (SOECs) for hydrogen production. The SOECs based on proton-conducting electrolytes, the proton-conducting SOECs (p-SOECs), can deliver pure hydrogen with some critical advantages over conventional oxide-ion conducting SOECs: reduced operating temperature, absence of nickel oxidation, and dry hydrogen production without the need for further separation [12–19]. Additionally, with the high proton conductivity of these conductors and the optimization of composition and fabrication, the electrolysis current density has been increasingly improved. Still, the development of electrolytes remains challenging due to a restrained total conductivity, chemical stability, and the electronic conduction under gas conditions which can reduce current efficiency [1, 16, 17, 20, 21]. Furthermore, consideration on potential electronic leakage during electrolysis operation, as found in recent works [16, 17, 21, 22], has become an additional concern that can be addressed by revealing the mechanism of the electronic conduction and developing new protonic ceramics. To better address these technical concerns, it is important to understand the underlying mechanism of proton conduction to promote innovations in electrolyte composition for practical operation at lower temperatures.

Proton conduction is a temperature-activated process and is observed in water-containing atmospheres as a function of gas atmosphere. Equation (1) shows the relationship of proton conductivity (σ_{OH^-} , S m⁻¹) with temperature following an Arrhenius type dependence,

$$\sigma_{\text{OH}^-} = \sigma_{\text{OH}^-}^* \exp\left(-\frac{E_a}{RT}\right) \quad (1)$$

where σ_{OH}^* is the pre-exponential factor describing proton conductivity ($S m^{-1}$), E_a is the activation energy for proton conduction (eV), k is the Boltzmann constant, and T is the temperature (K).

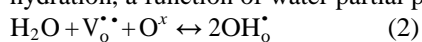
Among several proton-conducting perovskites developed in the past decades, doped BaCeO₃ and BaZrO₃ have shown the most promising application potential due to their high proton conductivity, chemical stability, and fabrication feasibility [5, 16, 23–27]. Perovskite systems containing Ce (BaCeO₃ and BaCe_{1-x}Zr_xO₃) exhibit high conductivity [23, 24, 28]. However, their low chemical stability in steam and CO₂ gas is a subject of concern [29–33]. In contrast, several studies have shown that BaZrO₃ is stable in steam and CO₂ and does not form BaCO₃ and Ba(OH)₂ phases [18, 34–38], unlike BaCeO₃ and BaCe_{1-x}Zr_xO₃ systems [29, 32, 39, 40]. Therefore, doped BaZrO₃ is a suitable material for p-SOECs applications and will be the subject of this mini review to illustrate the proton conduction phenomena.

BaZrO₃ doped with Y, Yb, In, Sc, Gd, Nd, Sm, etc have been extensively investigated as electrolytes that demonstrate considerable proton conductivity with optimized dopant element and concentration [5, 25, 26]. Several researchers have reported that the dopant and its concentration can considerably affect the proton conductivity of such materials [5, 25, 26]. Moreover, correlations between dopant atomic radius [25, 26] and electronegativity [41] with hydration energies and conductivities had been reported. Among doped BaZrO₃ compounds, 20% Y-doped BaZrO₃ has the highest conductivity to date [5, 25, 42]. However, there is a lack of comprehensive studies of doped BaZrO₃ to characterize the differences between proton concentration and mobility with temperature and gas conditions. Meanwhile the pursuit of other possible compositions based on BaZrO₃ perovskites is still ongoing to achieve higher conductivity.

This mini review will present the fundamental effects of defects location in material hydration and proton conduction. First, hydration thermodynamics for doped BaZrO₃ materials and the effect of doping on hydration and proton defect formation are reviewed. Second, proton localization in the lattice, particularly with respect to oxygen vacancies and dopant atoms, and the effect on proton concentration and mobility are presented in the context of defect associations and proton trapping phenomena. Finally, we present the implications of electronic conduction and strategies and future directions for further studies of proton-conducting materials.

2. Thermodynamics of hydration in proton conductors

The study of hydration thermodynamics is important for the characterization of new proton-conducting materials because hydration ability determines proton concentration under specific gas conditions and temperatures. Protons are incorporated into the material through the hydration of oxygen vacancies ($V_o^{\bullet\bullet}$), as shown in equation (2). The oxygen vacancies are usually created by doping the B-site of the perovskite (ABO₃) with a trivalent element (M) (equation (3)), and their concentration corresponds to half the dopant concentration. The hydration of oxygen vacancies in equation (2) is key as it determines the proton concentration ($[OH_o^*]$, % mol) of the material, which is a function of temperature, and under incomplete hydration, a function of water partial pressure (P_{H_2O})



Favorable hydration thermodynamics can be used as a guide for proton conduction as it is related to proton concentration as function of temperature. In this section, the basics of the hydration thermodynamics are reviewed, followed by a discussion about the incomplete hydration regime.

Table 1. ΔH_{hyd} and ΔS_{hyd} of various doped BaZrO₃.

Material	ΔH_{hyd} (kJ mol ⁻¹)	ΔS_{hyd} (J mol ⁻¹ K ⁻¹)	Reference
BaZr _{0.9} Y _{0.1} O _{3-δ}	-79.4	-88.8	[5]
BaZr _{0.8} Y _{0.2} O _{3-δ}	-93.3	-103.2	[5]
BaZr _{0.8} Y _{0.2} O _{3-δ}	-22	-39	[50]
BaZr _{0.7} Y _{0.3} O _{3-δ}	-26	-44	[50]
BaZr _{0.6} Y _{0.4} O _{3-δ}	-26	-41	[50]
BaZr _{0.9} Sc _{0.1} O _{3-δ}	-119.4	-124.9	[5]
BaZr _{0.8} Sc _{0.2} O _{3-δ}	-96	-104	[51]
BaZr _{0.9} Gd _{0.1} O _{3-δ}	-66.1	-85.9	[5]
BaZr _{0.9} In _{0.1} O _{3-δ}	-66.6	-90.2	[5]
BaZr _{0.9} In _{0.1} O _{3-δ}	-67	-90	[52]
BaZr _{0.5} In _{0.5} O _{3-δ}	-60	-95	[52]
BaZr _{0.25} In _{0.75} O _{3-δ}	-74	-109	[52]

The thermodynamics of the hydration reaction, equation (2), determines the proton concentration of the material as a function of temperature. The formation of the proton defect is governed by the equilibrium constant of the hydration reaction (K_{hyd}), equation (4)

$$[\text{OH}_o^*]^2$$

$$K_{\text{hyd}} = \frac{[\text{H}_2\text{O}]_o}{[\text{V}^{**}][\text{O}^R]} \quad (4)$$

K_{hyd} is then related to the Gibbs free energy of hydration (ΔG_{hyd}) according to equation (5), while ΔG_{hyd} is related to the enthalpy (ΔH_{hyd}) and entropy (ΔS_{hyd}) of hydration according to equation (6). Therefore, ΔH_{hyd} and ΔS_{hyd} can be calculated from knowing K_{hyd} as a function of temperature through the Van't Hoff equation, as shown in equation (7)

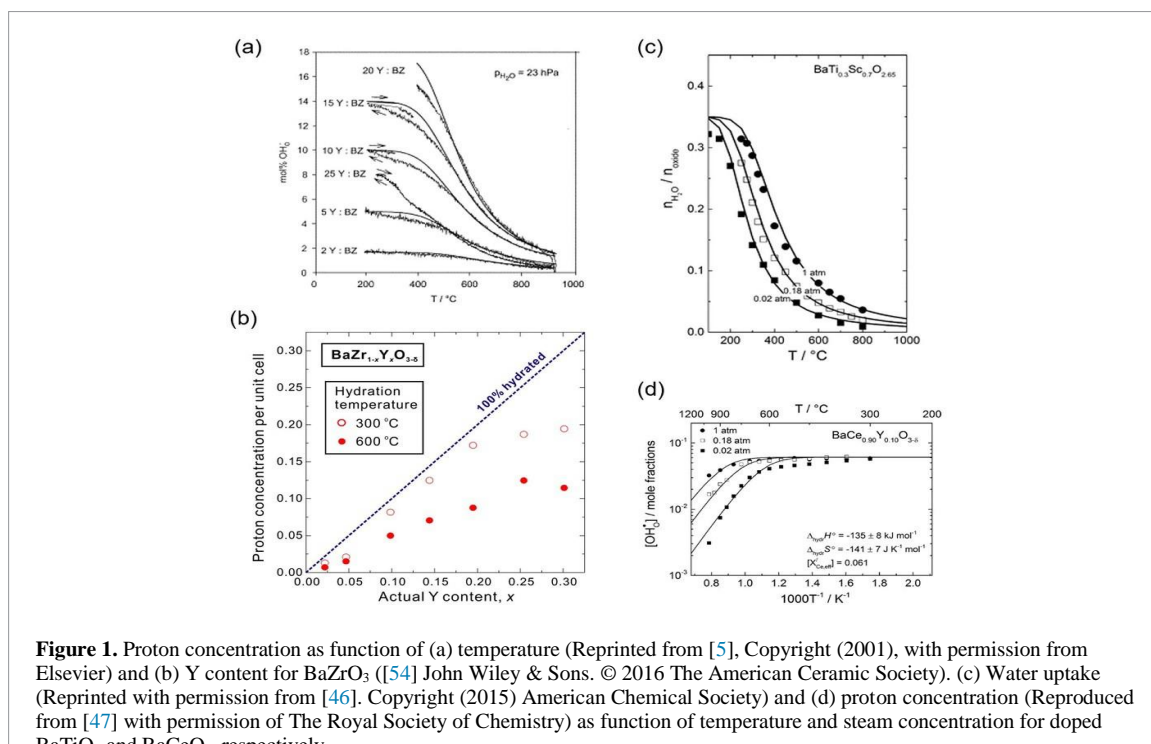
$$\Delta G_{\text{hyd}} = -RT \ln K_{\text{hyd}} \quad (5)$$

$$\Delta G_{\text{hyd}} = \Delta H_{\text{hyd}} - T\Delta S_{\text{hyd}} \quad (6)$$

$$\frac{\ln K}{\Delta H_{\text{hyd}}} = -\frac{1}{R} + \frac{\Delta S_{\text{hyd}}}{RT} \quad (7)$$

Favorable hydration thermodynamics is often characterized by a highly exothermic ΔH_{hyd} , a less negative ΔS_{hyd} , and a negative ΔG_{hyd} . Materials with more exothermic heats of hydration favor higher degrees of hydration as temperature rises [43]. The entropic impact of hydration is related to lattice ordering due to proton incorporation [5], which results in lattice expansion upon hydration and includes configuration and vibrational contributions [44]. In general, a less negative value of ΔS_{hyd} usually results in greater retention of protons at higher temperatures [44, 45]. Studies of doped BaZrO₃ hydration thermodynamics have correlated ΔH_{hyd} with the electronegativity of the dopant and tolerance factor of the material [41, 46, 47]. As the tolerance factor and electronegativity of the dopant decreases, ΔH_{hyd} tends to be more exothermic [47]. The effects of the dopant and its concentration on ΔH_{hyd} and ΔS_{hyd} are summarized in table 1. The values of ΔH_{hyd} and ΔS_{hyd} are dependent on the dopant, decreasing in hydration energy as follows: Gd > In > Y, with Sc-doped BaZrO₃ exhibiting the most favorable ΔH_{hyd} . However, ΔH_{hyd} and ΔS_{hyd} do not show any clear dependence on dopant concentration. Differences in the values of the hydration energy between references for a same material correspond to possible non-linear hydration isobars in all temperature ranges ascribed to defect interactions [48, 49] or to the formation of electronic species [50].

An important feature that results from studying the hydration of a material is the characterization of proton concentration with temperature. The hydration limit of doped BaZrO₃ frequently corresponds to the theoretical level of the dopant concentration [M]. Proton concentration as a function of temperature has been reported for numerous doped BaZrO₃ where the proton concentration reaches a maximum value at a low temperature and follows a decreasing trend with increasing temperature, as shown in figure 1(a). Proton concentration is normally studied through thermogravimetric analysis by correlating the weight increase from water uptake to the proton concentration, usually while studying hydration thermodynamics. Nuclear magnetic resonance (NMR) [53] has also been used to quantify the proton concentration. The application of these materials for p-SOECs requires operating temperatures in the range of 400 °C–600 °C, i.e. in the incomplete hydration regime, as seen in figures 1(a) and (b). A thoughtful characterization of the incomplete



hydration regime becomes essential to determine optimum doping concentrations. However, there are not many studies exploring this relationship. Moreover, in the incomplete hydration regime, proton concentration is a function of steam concentration [46, 47], as seen in figures 1(c) and (d) for other perovskites. Figures 1(c) and (d) suggest that proton concentration increases as steam concentration increases, although the effect is more significant in the low steam concentration region. Future studies on the proton concentration in doped BaZrO₃ as a function of steam concentration and temperature should reveal the dynamic of material hydration. It is worth pointing out that BaZrO₃-based electrolytes are refractory materials that require high sintering temperatures. To reduce the sintering temperature and improve densification, sintering aids (NiO [55–57], ZnO [58–61], CuO [55, 62], CaO [63], BaO–B₂O₃ [64], BaY₂NiO₅ [65], etc) have been used to facilitate densification by introducing a liquid phase for grain growth [66]. However, recent studies have shown that sintering aids have negative impact on the proton concentration [67–69], thus reducing conductivity. In addition, the sintering aids favor the detrimental formation of Ba-vacancies [67, 68] and the formation of undesired secondary phases in Y-doped BaZrO₃ [69–71]. Therefore, it is important to minimize the use of sintering aids or adopt other strategies for the material densification to suppress the impact of sintering aids on the conductivity.

Based on K_{hyd} and the hydration energies, lower temperatures and higher steam concentrations are favorable for the hydration of oxygen vacancies. A higher concentration of oxygen vacancies increases the proton concentration. The doping of the Zr-site is the most common strategy to create oxygen vacancies but Ba-site doping has also been explored [72–74]. The oxidizing character of the steam carrier gas is another important factor to consider during hydration as the oxidation of oxygen vacancies at certain experimental conditions [75, 76] could decrease the effective concentration of oxygen vacancies that can be hydrated. The effects of oxygen vacancies and dopant atoms in the material hydration will be discussed in the following sections.

3. Effect of oxygen vacancies and defects association on hydration and proton concentration

The location of oxygen vacancies and the extent of defect association are a representation of the chemical environment differences caused by dopants and their concentration. These differences are manifested in the hydration energies and, consequently, in proton concentration. While it has been suggested that oxygen

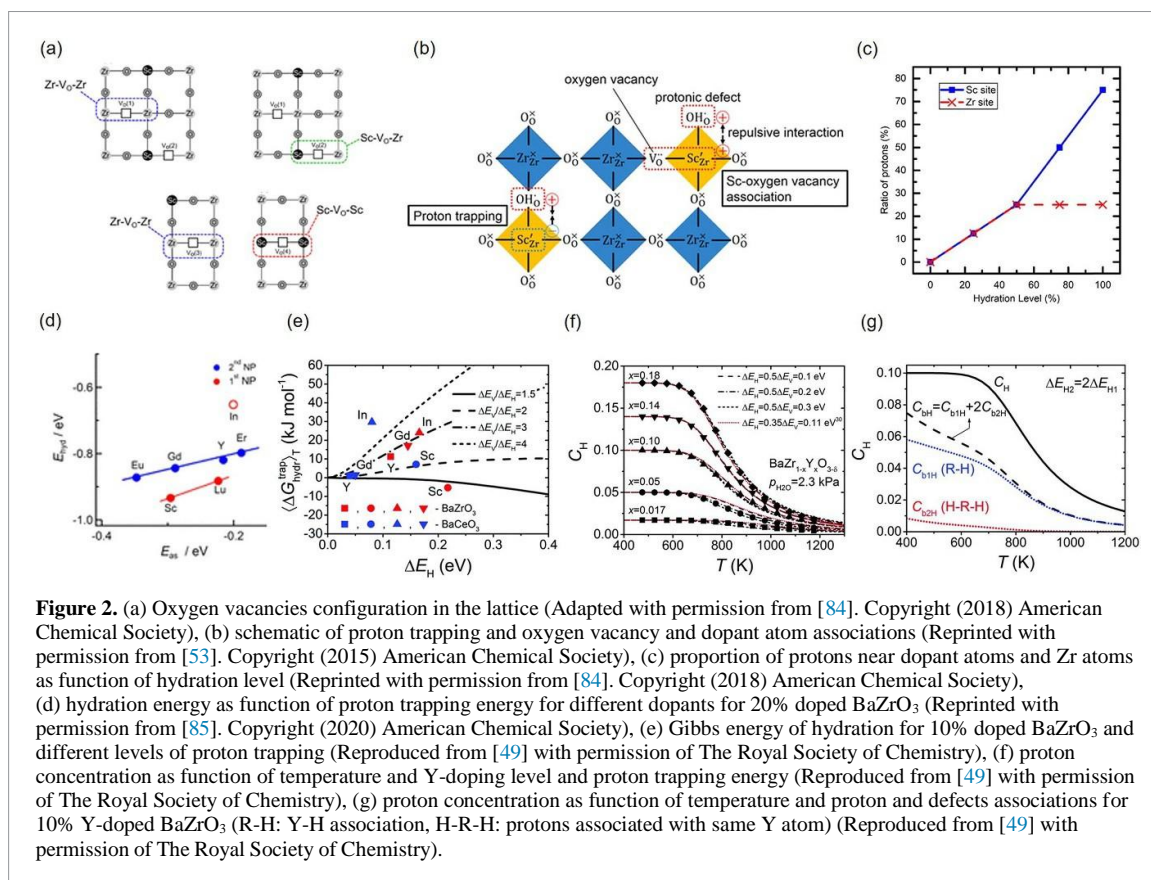


Figure 2. (a) Oxygen vacancies configuration in the lattice (Adapted with permission from [84]. Copyright (2018) American Chemical Society), (b) schematic of proton trapping and oxygen vacancy and dopant atom associations (Reprinted with permission from [53]. Copyright (2015) American Chemical Society), (c) proportion of protons near dopant atoms and Zr atoms as function of hydration level (Reprinted with permission from [84]. Copyright (2018) American Chemical Society), (d) hydration energy as function of proton trapping energy for different dopants for 20% doped BaZrO₃ (Reprinted with permission from [85]. Copyright (2020) American Chemical Society), (e) Gibbs energy of hydration for 10% doped BaZrO₃ and different levels of proton trapping (Reproduced from [49] with permission of The Royal Society of Chemistry), (f) proton concentration as function of temperature and Y-doping level and proton trapping energy (Reproduced from [49] with permission of The Royal Society of Chemistry), (g) proton concentration as function of temperature and proton and defects associations for 10% Y-doped BaZrO₃ (R-H: Y-H association, H-R-H: protons associated with same Y atom) (Reproduced from [49] with permission of The Royal Society of Chemistry).

vacancies tend to form in the vicinity of dopant atoms [53, 77], different configurations of oxygen vacancies can exist. Several works have successfully probed the localization of oxygen vacancies and protons at different configurations in doped BaZrO₃ by using specialized techniques such as neutron spin-echo [78], x-ray absorption spectroscopy [52], quasielastic neutron scattering [79, 80], Fourier transform infrared spectroscopy [81–83], and NMR [53, 84]. Some of those configurations correspond to oxygen vacancies in between Zr atoms ($Zr - V^{\bullet} - Zr$), between a Zr atom and a dopant atom ($Zr - V^{\bullet} - M$), and in between dopant atoms ($M - V^{\bullet} - M$) [84], as represented schematically in figure 2(a). The distribution of such configurations can be a function of the dopant atom and its concentration as a result of charge compensation during the formation of oxygen vacancies (equation (3)). On the other hand, positively charged protons and oxygen vacancies can associate with negatively charged dopant atoms [53], as seen in figure 2(b), for which the extent of such associations is a function of the dopant [77]. In this section, the oxygen vacancy location and defect associations will be used to discuss the hydration energy and proton concentration of doped BaZrO₃. The location of oxygen vacancies before their hydration has an impact on hydration energy. Consequently, oxygen vacancies near dopant atoms can be part of defect associations that can modify the hydration thermodynamics and the treatment of experimental data about the material hydration [48, 49]. Computational works have shown that the hydration energy of each configuration is different, suggesting that the experimental hydration energies are an average of all the different hydration energies for all the oxygen vacancy configurations [84, 86]. Additionally, some attempts to link the extent of hydration to the location of oxygen vacancies have been made by relating the stability of oxygen vacancies with their hydration abilities [84]. For example, density functional theory (DFT) of Sc-doped BaZrO₃ showed that the stability of oxygen vacancies depends on its location, being more stable near Sc atoms in comparison with oxygen vacancies near Zr atoms [84]. Consequently, the less stable oxygen vacancies are easier to hydrate than the more stable oxygen vacancies [84, 87]. This is significant as the hydration of some oxygen vacancies could result in protons in proton trapping positions. However, a Sc-NMR study on the hydration of Sc-doped BaZrO₃ revealed that at low proton concentrations, i.e. low material hydration due to high temperature, the protons were located equally near the Sc and Zr atoms [53, 84]. But as the proton concentration

increased, i.e. a material hydration increased by low temperatures, most of the protons were located near Sc [53, 84], as seen in figure 2(c).

The association of a proton with a dopant atom is referred to as proton trapping. DFT studies have correlated hydration energy with proton trapping energy for different dopants in BaZrO₃. The results suggested that high proton trapping energy led to more exothermic hydration energies [85], as shown in figure 2(d). However, another DFT study suggested that proton trapping can enhance or inhibit the hydration of the material [49], as can be observed from figure 2(e) where the Gibbs free energy of hydration is presented as a function of the proton association energies. Such boundaries depend on the dopant and its concentration, as well as the trapping energy for the proton and for the oxygen vacancies with the dopant [49]. As shown in figures 2(d) and (e), as defect associations affect hydration equilibrium, failing to include these associations in the data analysis of hydration measurements could affect the calculation of proton concentrations [48, 49, 85, 88]. As seen in figure 2(f), at higher doping concentration for Y-doped BaZrO₃, the proton concentration does not reach the theoretical values at the low temperature region [49].

Additionally, the overall proton concentration could be divided between the un-associated protons and trapped protons [49], as seen in figure 2(g). The effect of trapped protons and unassociated protons on proton conduction will be reviewed next. Nonetheless, the complexity added by defect association on proton concentration must be understood as the search for the optimum dopant and doping concentration of BaZrO₃ continues.

4. Proton conduction in solid oxides

It is well recognized that protons diffuse through solid oxides by the Grotthuss mechanism. Proton diffusion involves the reorientation of a proton towards a neighboring oxygen atom and the jump of the proton towards the neighboring oxygen atom [41, 89], as shown in figure 3(a). The proton jump step is mostly considered as the rate limiting step [41, 89]. Due to the nature of the Grotthuss mechanism, the characteristics of the O–H bond become important in the understanding of proton conduction in perovskites. The O–H bond can be stretched, shortened, and reoriented due to the atoms around it, changing in strength accordingly [82]. Normally, when the O–H bond is stronger, the rate of reorientation decreases and proton transfer increases [82]. Oxygen vacancies and dopant atoms can modify the O–H bond strength. For example, it was reported that as the oxygen vacancies and dopant atoms influence a repulsive and attractive force around the proton due to their positive and negative charge, respectively, the proton tilts towards a neighboring oxygen and hence stronger O–H bonds are created [82]. The overall effect is observed in the increase in the proton jump step at the expense of slowing the reorientation step [41, 82], modifying the activation energy for proton diffusion. Moreover, the B–H interaction can also contribute to the activation energy of proton diffusion as the repulsive interaction between a proton and the host atom B inhibits the formation of a linear O–H bond, resulting in an increase of activation energy for proton transfer [41, 45, 90]. The B–H interaction can be modified by doping resulting in changes in the basicity of the oxygen atoms and in the activation energy for proton diffusion [41, 90].

Proton diffusion from the surface to the bulk of the material could represent an important energy barrier, as suggested by DFT studies in proton conductor oxides [87, 91]. As seen in figure 3(b), the energy barriers for the initial proton jump (I and T in figure 3(b)) are higher than the energy barrier for proton jumps away from the surface [91]. Additionally, the study of the material surface and its space charge region is relevant for the study of the hydration process [87, 92]. Proton diffusion into the bulk requires the counter diffusion of oxygen vacancies from the bulk to the surface, and therefore, the predicted depletion or segregation of oxygen vacancies (figure 3(c)) could increase the energy barriers for proton diffusion from the surface to the bulk of the material. Thorough studies about the energy barriers on proton diffusion from the surface to the bulk in doped BaZrO₃ could help explain the differences in conductivity observed experimentally for different dopants.

Proton conductivity is proportional to proton mobility (μ_{OH^-} , $\text{m}^2 \text{V}^{-1} \text{s}^{-1}$) and proton diffusivity

(D_{OH^-} , $\text{m}^2 \text{s}^{-1}$) according to equations (8) and (9), respectively,

$$\sigma_{\text{OH}^-} =$$

$$\frac{z_{\text{OH}^-} F [\text{OH}_o^{\bullet}] \mu_{\text{OH}^-}}{V_M} \quad (8)$$

$$\frac{z_{\text{OH}^-}^2 \cdot f^2 [\text{OH}_o^{\bullet}] D_{\text{OH}^-}}{\sigma_{\text{OH}^-}^{\text{OH}_o^{\bullet}}}$$

$$V_M RT$$

(9)

where $z_{\text{OH}_5^-}$ is the proton charge, F is the Faraday constant, V_M is the molar volume of the ceramic ($\text{m}^3 \text{mol}^{-1}$), and R is the gas constant. D_{OH^-} and μ_{OH^-} are related through the Nernst–Einstein equation, as shown in equation (10)

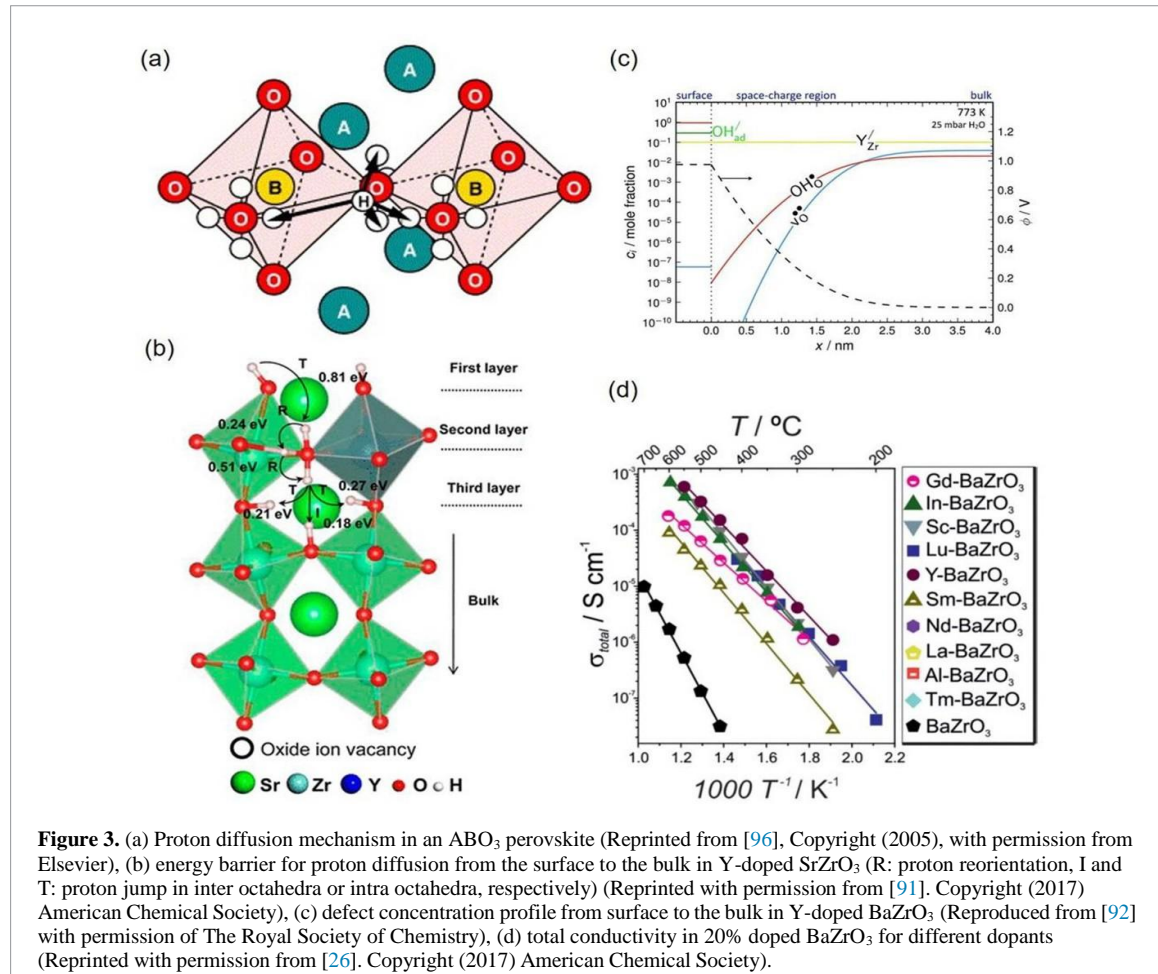


Figure 3. (a) Proton diffusion mechanism in an ABO₃ perovskite (Reprinted from [96], Copyright (2005), with permission from Elsevier), (b) energy barrier for proton diffusion from the surface to the bulk in Y-doped SrZrO₃ (R: proton reorientation, I and T: proton jump in inter octahedra or intra octahedra, respectively) (Reprinted with permission from [91], Copyright (2017) American Chemical Society), (c) defect concentration profile from surface to the bulk in Y-doped BaZrO₃ (Reproduced from [92] with permission of The Royal Society of Chemistry), (d) total conductivity in 20% doped BaZrO₃ for different dopants (Reprinted with permission from [26], Copyright (2017) American Chemical Society).

Table 2. Activation energy, E_a , and total conductivity in wet reducing or inert gas, σ_{total} , at 600 °C of various doped BaZrO₃.

Material	E_a (eV)	Reference	σ_{total} (S cm ⁻¹)	Reference
BaZr _{0.9} Y _{0.1} O _{3-δ}	0.43	[5]	—	
BaZr _{0.8} Y _{0.2} O _{3-δ}	0.48	[5]	0.004 0.0125	[93, 94]
BaZr _{0.7} Y _{0.3} O _{3-δ}	—		0.0011	[93]
BaZr _{0.6} Y _{0.4} O _{3-δ}	—		0.0007	[93]
BaZr _{0.9} Sc _{0.1} O _{3-δ}	0.50	[5]	—	
BaZr _{0.8} Sc _{0.2} O _{3-δ}	0.50	[51]	0.005	[51]
BaZr _{0.9} Gd _{0.1} O _{3-δ}	0.47	[5]	—	
BaZr _{0.8} Gd _{0.2} O _{3-δ}	—		0.0002	[26]
BaZr _{0.9} In _{0.1} O _{3-δ}	0.48	[5]	—	
BaZr _{0.8} In _{0.2} O _{3-δ}	—		0.0006	[95]
BaZr _{0.5} In _{0.5} O _{3-δ}	0.62	[52]	—	
BaZr _{0.25} In _{0.75} O _{3-δ}	0.40	[52]	—	
BaZr _{0.8} Sm _{0.2} O _{3-δ}	—		0.00009	[26]

$$\frac{\mu_{\text{OH}_5^-}}{RT} = \frac{z_{\text{OH}_5^-} F}{RT} \phi \quad (10)$$

The activation energies (see equation (1)) obtained from conductivity measurements are frequently reported and

table 2 shows the activation energy of various doped BaZrO₃ with all materials in the range of 0.4–0.6 eV. As seen in table 2, the choice of dopant and dopant concentration can modify the activation energy for proton conduction. For example, the activation energies from the same study at 10% doping are 0.43 eV for Y, 0.50 eV for Sc, 0.48 eV for In, and 0.47 eV for Gd [5]. Additionally, the effect of the dopant choice on proton diffusivity can be appreciated in figure 3(d) where the conductivity differences are about two orders of

magnitude for different dopants [26] and on table 2 where representative conductivities at 600 °C are shown.

Consequently, understanding the proton conduction phenomena and how different materials and material doping can modify proton conduction is central to advancing proton-conducting materials research.

It is worth mentioning that the conduction of oxygen ions (or V_O^{••}) can also exist in proton-conducting oxides. Some studies have shown oxygen ion conduction at low oxygen partial pressures and dry conditions [97–99] at increased temperature, usually above 700 °C [100, 101]. This mixed proton and oxygen ion conduction in the electrolyte has been reported to be beneficial for solid oxide cells. For example, studies have shown an increase of efficiencies in fuel cell operation [23, 102, 103] and, when steam is added to both electrodes in electrolysis operation, an increase on the hydrogen production due to the simultaneous water electrolysis on both electrodes [19]. Nevertheless, it should be considered that the gain of additional oxygen ion conduction does not diminish the proton conductivity due to the conditions necessary for the oxygen ion conduction.

5. Proton trapping and its effect on proton transport

Proton trapping reduces the proton mobility and is manifested in the increase of activation energy for proton conduction at lower temperatures [88]. At low temperatures, the protons do not have enough energy to move from the trapping positions, hence the nonlinearity of the activation energy seen for this temperature range. This phenomenon has been receiving increased attention as some material applications require an operating temperature range that could fall under the proton trapping regime. Evidence of proton trapping requires the probing of proton position near dopant atoms. However, computational methods have predicted proton trapping conditions. Figure 4(a) shows a schematic representation of proton binding energies for Y-doped BaZrO₃ for different proton configurations, where the proton configuration in between two Y atoms has the highest binding energy [104].

In section 3 it was pointed out that increasing doping concentration increases proton trapping. Nonetheless, computational work has found that as proton trapping increases due to higher proton concentration there is a point where the trapped protons prevent other protons from being trapped and percolation channels form due to the overlap of trapping zones, and hence the proton mobility increases again [105, 106]. However, the doping concentration for the formation of percolation channels could be dependent on the dopant element. Additionally, proton-proton interactions could have a negative effect on proton mobility with increasing proton concentration due to their repulsive interaction [106]. However, in 20% Y-doped BaZrO₃, such negative interactions are not dominant, and instead, the trapped protons enhance the proton mobility of the free protons by filling the trapping positions [106].

Defect associations also have an effect on proton trapping. Oxygen vacancies and dopant atoms can form an association that could prevent the trapping effect (figure 2(b)) [53, 77]. On the other hand, the dopant-dopant association can modify transport properties of the material and could enhance proton trapping [107]. A DFT study looking at Y–Y defect associations and their effect on proton trapping on Y-doped BaZrO₃ suggested that a triangular configuration of Y associations is responsible for the proton trapping phenomena observed in Y-doped BaZrO₃ [107], as shown in figure 4(b). For Y-doped BaZrO₃, studies have suggested that the Y–Y associations increase with doping concentration [107, 108].

Finally, doping concentration and dopant element choice yield varied effects on proton trapping.

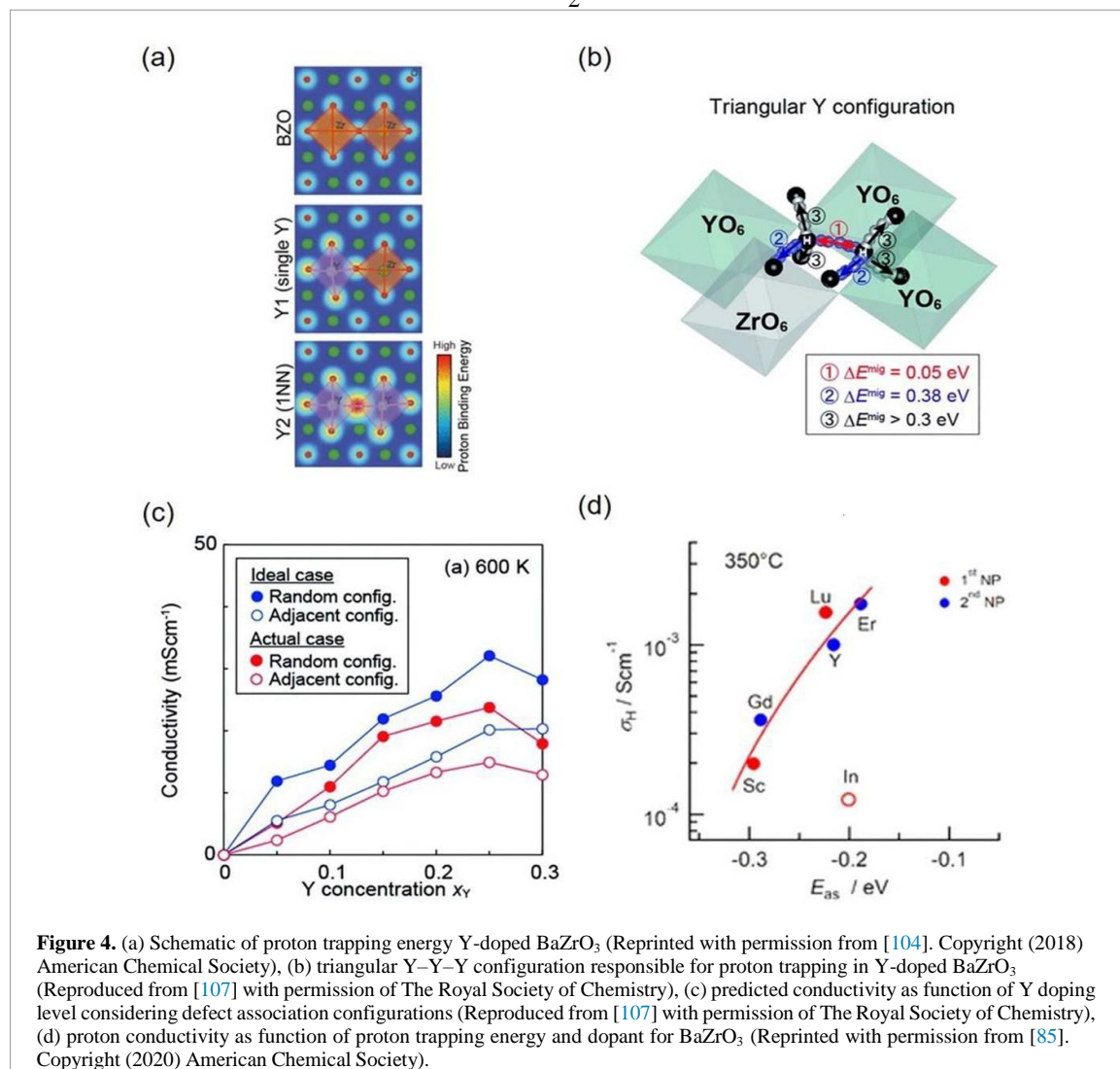
Figure 4(c) shows conductivity as a function of Y doping concentration, and it can be observed that there is an optimum concentration where conductivity is maximized [107]. However, the ideal doping level for different elements may not necessarily be the same. Figure 4(d) shows proton conductivity as a function of proton trapping for different dopant elements for BaZrO₃, where the correlation shows that for favorable proton trapping energies the proton conductivity decreases [85]. Amid all these transport phenomena, the analysis of proton conductivity at specific operating conditions should be carefully considered and a balance between doping concentration, proton concentration, and proton mobility is essential.

6. Electronic conduction in solid oxides

In addition to the proton conduction of BaZrO₃-based electrolytes, electronic defects such as hole defects (h[•]) are formed by the oxidation of oxygen vacancies according to equation (11). Hole defects can be considered a main charge carrier under certain experimental conditions, typically under high oxygen partial pressures and dry conditions [2, 99, 109]. Therefore, the implications of electronic conduction in solid oxides are

briefly discussed
 $O + V^{**} \leftrightarrow O^x + 2h^{\cdot}$ (11)

$$\frac{1}{2} \quad 2 \quad o \quad o$$



The main concern for electronic conduction is related to the electronic leakage in p-SOECs, where such leakage decreases the Faradaic efficiency [10, 17, 21]. Several advances have been made towards the understanding of hole conduction, such as the development of defect chemistry and transport models that highlight the conditions benefitting hole formation and conduction [17, 21, 110–113].

The effect of electronic defects on material hydration has also been studied. Theoretical models have suggested that electronic defects have the potential to modify the material hydration by the formation of deep acceptor states [75, 76]. Additionally, the nonlinearity of the hydration isobars has been attributed to electronic defect formation [50]. Experimental studies have also shown a two-fold proton diffusion from the surface to the bulk of the material under high temperatures and high oxygen partial pressures suggesting that the hole conduction decouples the diffusion of protons and oxygen vacancies [114, 115]. Thus, the dominance of oxygen vacancy hydration over oxidation is critical to the understanding of material hydration and subsequent proton and electronic conduction in solid oxides.

7. Concluding remarks and prospects

As discussed in this mini review, attention must be given not only to the choice of dopant but also to its concentration. High doping concentrations can be strategic for improving proton concentration, as presented by a recent work in Sc-doped BaZrO₃ [51]. While the effect of percolation channels for proton conduction and different defect associations can be further explored for high doping materials, some problematic aspects of high concentration of dopants such as phase stability and sinterability should be considered.

A comprehensive study of the effects of the gas condition on proton conduction in these materials is necessary.

The underlying mechanism responsible for proton conductivity differences as a function of the gas condition remains unclear for the most part, especially when it comes to how proton conduction is affected by high steam concentrations and highly oxidizing atmospheres. Hence, the effect of gas conditions on the thermodynamics and transport phenomena should be thoroughly considered.

Finally, coupling advanced characterization techniques with simulations could enhance the understanding of proton conduction mechanisms, particularly proton formation and diffusion. By inputting proton conduction parameters, the developed models will be able to predict relevant p-SOECs properties such as proton current density and efficiency as a function of operating conditions.

References

- [1] Iwahara H, Esaka T, Uchida H and Maeda N 1981 Proton conduction in sintered oxides and application to steam electrolysis for hydrogen production *Solid State Ion.* **3/4** 359–63
- [2] Uchida H, Maeda N and Iwahara H 1983 Relation between proton and hole conduction in SrCeO₃-based solid electrolytes underwater-containing atmospheres at high temperatures *Solid State Ion.* **11** 117–24
- [3] Haugrud R and Norby T 2006 Proton conduction in rare-earth ortho-niobates and ortho-tantalates *Nat. Mater.* **5** 193–6
- [4] Fop S, McCombie K S, Wildman E J, Skakle J M S, Irvine J T S, Connor P A, Savaniu C, Ritter C and McLaughlin A C 2020 High oxide ion and proton conductivity in a disordered hexagonal perovskite *Nat. Mater.* **19** 752–7
- [5] Kreuer K D, Adams S, Munch W, Fuchs A, Klock U and Maier J 2001 Proton conducting alkaline earth zirconates and titanates for high drain electrochemical applications *Solid State Ion.* **145** 295–306
- [6] Ding D, Zhang Y, Wu W, Chen D, Liu M and He T 2018 A novel low-thermal-budget approach for the co-production of ethylene and hydrogen via the electrochemical non-oxidative deprotonation of ethane *Energy Environ. Sci.* **11** 1710–6
- [7] Iwahara H, Asakura Y, Katahira K and Tanaka M 2004 Prospect of hydrogen technology using proton-conducting ceramics *Solid State Ion.* **168** 299–310
- [8] Li M, Hua B, Wang L, Sugar J D, Wu W, Ding Y, Li J and Ding D 2021 Switching of metal–oxygen hybridization for selective CO₂ electrohydrogenation under mild temperature and pressure *Nat. Catal.* **4** 274–83
- [9] Iwahara H 1995 Technological challenges in the application of proton conducting ceramics *Solid State Ion.* **77** 289–98
- [10] Duan C *et al* 2018 Highly durable, coking and sulfur tolerant, fuel-flexible protonic ceramic fuel cells *Nature* **557** 217–22
- [11] Wu W, Ding H, Zhang Y, Ding Y, Katiyar P, Majumdar P K, He T and Ding D 2018 3D self-architected steam electrode enabled efficient and durable hydrogen production in a proton-conducting solid oxide electrolysis cell at temperatures lower than 600 °C *Adv. Sci.* **5** 1800360
- [12] Irvine J T S, Neagu D, Verbraeken M C, Chatzichristodoulou C, Graves C and Mogensen M B 2016 Evolution of the electrochemical interface in high-temperature fuel cells and electrolyzers *Nat. Energy* **1** 15014
- [13] Zhan Z, Bierschenk D M, Cronin J S and Barnett S A 2011 A reduced temperature solid oxide fuel cell with nanostructured anodes *Energy Environ. Sci.* **4** 3951–4
- [14] Wu J, Johnson C D, Gemmen R S and Liu X 2009 The performance of solid oxide fuel cells with Mn–Co electroplated interconnect as cathode current collector *J. Power Sources* **189** 1106–13
- [15] Tao S W, Irvine J T S and Kilner J A 2005 An efficient solid oxide fuel cell based upon single-phase perovskites *Adv. Mater.* **17** 1734–7
- [16] Duan C, Kee R, Zhu H, Sullivan N, Zhu L, Bian L, Jennings D and O'Hayre R 2019 Highly efficient reversible protonic ceramic electrochemical cells for power generation and fuel production *Nat. Energy* **4** 230–40
- [17] Choi S, Davenport T C and Haile S M 2019 Protonic ceramic electrochemical cells for hydrogen production and electricity generation: exceptional reversibility, stability, and demonstrated faradaic efficiency *Energy Environ. Sci.* **12** 206–15
- [18] Duan C, Tong J, Shang M, Nikodemski S, Sanders M, Ricote S, Almansoori A and O'Hayre R 2015 Readily processed protonic ceramic fuel cells with high performance at low temperatures *Science* **349** 1321–6
- [19] Kim J, Jun A, Gwon O, Yoo S, Liu M, Shin J, Lim T-H and Kim G 2018 Hybrid-solid oxide electrolysis cell: a new strategy for efficient hydrogen production *Nano Energy* **44** 121–6
- [20] Dippon M, Babinić S M, Ding H, Ricote S and Sullivan N P 2016 Exploring electronic conduction through BaCe_xZr_{0.9-x}Y_{0.1}O_{3-d} proton-conducting ceramics *Solid State Ion.* **286** 117–21
- [21] Völlestad E, Strandbakke R, Tarach M, Catalan-Martinez D, Fontaine M L, Beeaff D, Clark D R, Serra J M and Norby T 2019
- [22] Mixed proton and electron conducting double perovskite anodes for stable and efficient tubular proton ceramic electrolyzers *Nat. Mater.* **18** 752–9
- [23] Ding H *et al* 2020 Self-sustainable protonic ceramic electrochemical cells using a triple conducting electrode for hydrogen and power production *Nat. Commun.* **11** 1907
- [24] Yang L, Wang S, Blinn K, Liu M, Liu Z, Cheng Z and Liu M 2009 Enhanced sulfur and coking tolerance of a mixed ion conductor for SOFCs: BaZr_{0.1}Ce_{0.7}Y_{0.2-x}Yb_xO_{3-δ} *Science* **326** 126–9
- [25] Choi S, Kucharczyk C J, Liang Y, Zhang X, Takeuchi I, Ji H-I and Haile S M 2018 Exceptional power density and stability at

- [28] intermediate temperatures in protonic ceramic fuel cells *Nat. Energy* **3** 202–10
- [29] Han D, Shinoda K, Sato S, Majima M and Uda T 2015 Correlation between electroconductive and structural properties of proton conductive acceptor-doped barium zirconate *J. Mater. Chem. A* **3** 1243–50
- [30] Gilardi E, Fabbri E, Bi L, Rupp J L M, Lippert T, Pergolesi D and Traversa E 2017 Effect of dopant–host ionic radii mismatch on acceptor-doped barium zirconate microstructure and proton conductivity *J. Phys. Chem. C* **121** 9739–47
- [31] Xie K, Yan R, Chen X, Dong D, Wang S, Liu X and Meng G 2009 A new stable BaCeO₃-based proton conductor for intermediate-temperature solid oxide fuel cells *J. Alloys Compd.* **472** 551–5
- [32] Murphy R, Zhou Y, Zhang L, Soule L, Zhang W, Chen Y and Liu M 2020 A new family of proton-conducting electrolytes for reversible solid oxide cells: BaHf_xCe_{0.8-x}Y_{0.1}Yb_{0.1}O_{3-δ} *Adv. Funct. Mater.* **30** 2002265
- [33] Zhang Y, Xie D, Chi B, Pu J, Li J and Yan D 2019 Basic properties of proton conductor BaZr_{0.1}Ce_{0.7}Y_{0.1}O_{3-δ} (BZCYYb) *material Asia-Pac. J. Chem. Eng.* **14** e2322
- [35] Qian J, Sun W, Shi Z, Tao Z and Liu W 2015 Chemically stable BaZr_{0.7}Pr_{0.1}Y_{0.2}O_{3-δ}-BaCe_{0.8}Y_{0.2}O_{3-δ} bilayer electrolyte for intermediate temperature solid oxide fuel cells *Electrochim. Acta* **151** 497–501
- [36] Yoo Y and Lim N 2013 Performance and stability of proton conducting solid oxide fuel cells based on yttrium-doped barium cerate-zirconate thin-film electrolyte *J. Power Sources* **229** 48–57
- [37] Reddy G S and Bauri R 2016 Y and In-doped BaCeO₃-BaZrO₃ solid solutions: chemically stable and easily sinterable protonconducting oxides *J. Alloys Compd.* **688** 1039–46
- [38] Medvedev D, Lyagaeva J, Plaksin S, Demin A and Tsiakaras P 2015 Sulfur and carbon tolerance of BaCeO₃-BaZrO₃ proton-conducting materials *J. Power Sources* **273** 716–23
- [39] Bi L, Shafi S P and Traversa E 2015 Y-doped BaZrO₃ as a chemically stable electrolyte for proton-conducting solid oxide electrolysis cells (SOECs) *J. Mater. Chem. A* **3** 5815–9
- [40] Fabbri E, Pergolesi D, d'Epifanio A, di Bartolomeo E, Balestrino G, Licoccia S and Traversa E 2009 Improving the performance of high temperature protonic conductor (HTPC) electrolytes for solid oxide fuel cell (SOFC) applications *Key Eng. Mater.* **421–422** 336–9
- [41] Sun W, Shi Z, Liu M, Bi L and Liu W 2014 An easily sintered, chemically stable, barium zirconate-based proton conductor for high-performance proton-conducting solid oxide fuel cells *Adv. Funct. Mater.* **24** 5695–702
- [43] Fabbri E, Depifanio A, Dibartolomeo E, Licoccia S and Traversa E 2008 Tailoring the chemical stability of Ba(Ce_{0.8-x}Zr_x)Y_{0.2}O_{3-δ} protonic conductors for intermediate temperature solid oxide fuel cells (IT-SOFCs) *Solid State Ion.* **179** 558–64
- [45] Bi L, Fabbri E, Sun Z and Traversa E 2011 Sinteractivity, proton conductivity and chemical stability of BaZr_{0.7}In_{0.3}O_{3-δ} for solid oxide fuel cells (SOFCs) *Solid State Ion.* **196** 59–64
- [47] Vahid Mohammadi A and Cheng Z 2015 Fundamentals of synthesis, sintering issues, and chemical stability of BaZr_{0.1}Ce_{0.7}Y_{0.1}O_{3-δ} proton conducting electrolyte for SOFCs *J. Electrochem. Soc.* **162** F803–11
- [48] Sawant P, Varma S, Wani B N and Bharadwaj S R 2012 Synthesis, stability and conductivity of BaCe_{0.8-x}Zr_xY_{0.2}O_{3-δ} as electrolyte for proton conducting SOFC *Int. J. Hydrog. Energy* **37** 3848–56
- [49] Kreuer K D 2003 Proton-conducting oxides *Annu. Rev. Mater. Res.* **33** 333–59
- [51] Yamazaki Y, Hernandez-Sanchez R and Haile S M 2009 High total proton conductivity in large-grained yttrium-doped barium zirconate *Chem. Mater.* **21** 2755–62
- [52] Larring Y and Norby T 1997 The equilibrium between water vapour, protons, and oxygen vacancies in rare earth oxide *Solid State Ion.* **97** 523–8
- [53] Bjørheim T S, Løken A and Haugsrud R 2016 On the relationship between chemical expansion and hydration thermodynamics of proton conducting perovskites *J. Mater. Chem. A* **4** 5917–24
- [54] Kreuer K D 1999 Aspects of the formation and mobility of protonic charge carriers and the stability of perovskite-type oxides *Solid State Ion.* **125** 285–302
- [56] Bjørheim T S, Rahman S M, Eriksson S G, Knee C S and Haugsrud R 2015 Hydration thermodynamics of the proton conducting oxygen-deficient perovskite series BaTi_{1-x}M_xO_{3-y/2} with M = In or Sc *Inorg. Chem.* **54** 2858–65
- [57] Løken A, Bjørheim T S and Haugsrud R 2015 The pivotal role of the dopant choice on the thermodynamics of hydration and associations in proton conducting BaCe_{0.9}X_{0.1}O_{3-δ} (X = Sc, Ga, Y, In, Gd and Er) *J. Mater. Chem. A* **3** 23289–98
- [58] Eisele S, Draber F M and Grieshammer S 2021 The effect of ionic defect interactions on the hydration of yttrium-doped barium zirconate *Phys. Chem. Chem. Phys.* **23** 4882–91
- [60] Putilov L P and Tsidilkovski V I 2019 Impact of bound ionic defects on the hydration of acceptor-doped proton-conducting perovskites *Phys. Chem. Chem. Phys.* **21** 6391–406
- [61] Yamazaki Y, Babilo P and Haile S M 2008 Defect chemistry of yttrium-doped barium zirconate: a thermodynamic analysis of water uptake *Chem. Mater.* **20** 6352–7
- [62] Hyodo J, Kitabayashi K, Hoshino K, Okuyama Y and Yamazaki Y 2020 Fast and stable proton conduction in heavily scandium-doped polycrystalline barium zirconate at intermediate temperatures *Adv. Energy Mater.* **10** 2000213
- [64] Giannici F, Longo A, Balerna A, Kreuer K-D and Martorana A 2009 Proton dynamics in In:BaZrO₃: insights on the atomic and electronic structure from x-ray absorption spectroscopy *Chem. Mater.* **21** 2641–9
- [65] Oikawa I and Takamura H 2015 Correlation among oxygen vacancies, protonic defects, and the acceptor dopant in Sc-doped BaZrO₃ studied by ⁴⁵Sc nuclear magnetic resonance *Chem. Mater.* **27** 6660–7